scientific reports

Check for updates

OPEN

MHC class I and II expression and induction in oligodendrocytes varies with age

Riley B. Catenacci[1,2], Danny Galleguillos[2], Adriana Rhodes[2], Sloan Phillips[2] & Peter A. Calabresi[1,2]✉

Oligodendroglia expressing major histocompatibility complex (MHC) molecules have become of central interest in multiple sclerosis (MS) research, but their role in aging is still being elucidated. Using MHC class I and II reporter mice, we compared oligodendroglial MHC expression in neonatal, young adult (8–16 weeks), and aging (52 weeks) mice at baseline and after stereotactic delivery of AAV-GFAP-IFNγ. We found that MHC class I-expressing oligodendroglia were present in both the naïve brain and spinal cord, while MHC class II-expressing oligodendroglia were seen only in the spinal cord of aging mice at baseline. After AAV injection, MHC expression in oligodendroglia increased, recapitulating pathology seen in MS mouse models and in MS post-mortem tissue. After IFNγ-AAV injection, the abundance of MHC class I-expressing oligodendroglia did not vary with age, whereas MHC class II-expressing oligodendroglia were more abundant in aging mice than neonatal and young adult mice. Our results suggest that MHC class II-expressing oligodendroglia are more prevalent with aging, which may contribute to the mechanisms underlying progressive MS and other age-related neurodegenerative diseases with central nervous system inflammation.

Multiple sclerosis (MS) onset and progression are age-related. The relapsing-remitting form of MS (RRMS) is most commonly diagnosed between the ages of 20 and 40, and transitions to secondary progressive disease (SPMS) within 25 years on average[1]. Primary progressive MS (PPMS), in which disability increases from the onset without remission, is commonly diagnosed in the same age range as SPMS, beginning in the mid-40s[1]. Later onset MS is associated with faster disease progression[1,2].

Given that progressive disease is associated with failed remyelination[3,4], attention has recently shifted to how aging affects cells of the oligodendroglial lineage. It is well established that oligodendrocyte progenitor (OPC) migration and differentiation declines with age, as does myelinogenesis by mature oligodendrocytes (OLs)[5]. These changes are driven by both intrinsic differences in aging cells as well as extrinsic factors such as extracellular matrix stiffening, the accumulation of senescent cells, and low-grade "inflammaging"[1,6,7].

Immune OPCs/OLs (iOPCs/OLs), characterized by expression of major histocompatibility complex (MHC) molecules, have been identified in MS mouse models and MS post-mortem tissue[8–12]. It has been suggested that these cells sit at the nexus of inflammatory and myelinating pathology seen in MS, and thus could be a viable therapeutic target[13]. However, much of the work examining iOPCs/iOLs has been executed in vitro, using neonatal mouse cells or human induced pluripotent stem cells that often have been epigenetically reprogrammed and lack features of cellular aging.

We previously developed beta 2 microglobulin-tdTomato (B2M-tdT) and cluster of differentiation 74-tDT (CD74-tdT) reporter mice to identify MHC class I and II-expressing cells, respectively. We observed that MHC-expressing oligodendroglia increased with disease severity and inflammatory infiltrate and were more prevalent in areas of increased inflammation in multiple mouse models of MS[9], suggesting that they are poised to play an active role in disease pathophysiology. These studies were limited to young adult mice between 10 and 16 weeks of age. Thus, it is unclear how age influences iOPC/OL induction, which could have important implications for MS.

Emerging evidence suggests that oligodendroglia may be more responsive to inflammation with aging. Response to IFNγ and antigen processing/presentation were two of the most significantly upregulated transcriptomic pathways in OPCs from 310-day-old mice compared to those from 12-day-old mice[14]. Proteomic data from de la Fuente et al. show that OLs from aged mice (13–15 months) express more immune-related proteins than young adults (3–4 months), including CD74, cathepsins, and C1q[15]. OLs from the brains of mice

[1]The Solomon H. Snyder Department of Neuroscience, Johns Hopkins University School of Medicine, Baltimore, MD 21205, USA. [2]Department of Neurology, Johns Hopkins University School of Medicine, Baltimore, MD 21287, USA. ✉email: pcalabr1@jhmi.edu

21–23 months old express higher levels of MHC class I and complement genes compared to those from young adults[16], and aging is associated with the activation of immune pathways in OPCs[17]. In addition, single cell sequencing of the subventricular zone of aged mice showed that OPCs and OLs express higher levels of IFNγ response transcripts despite equal expression of IFNγ receptors[18]. Finally, an increase in CD8 + T cells in the white matter of the aging brain has been shown to induce IFNγ-related proteins, including B2M and STAT1 in OLs[19]. However, these studies did not directly compare oligodendroglia in mice of different ages under inflammatory conditions.

To determine if changes in oligodendroglial response to inflammation with age mirror age-related changes observed in MS, we compared oligodendroglial MHC expression in our MHC reporter mice under basal and inflammatory conditions in different age groups: neonatal mice, representing a developmental age in humans; young adult (8–16 weeks), corresponding with the age of RRMS onset in humans[20]; and aging (52–56 weeks), corresponding with the age of PMS onset[20].

Results

MHC class II-, but not class I-, expressing oligodendroglia show age specificity in the naïve CNS

We first sought to determine if the presence of MHC-expressing oligodendroglia varies with age at baseline using our previously validated tdTomato (tdT) reporter mouse lines that allow detection of MHC class I (MHCI-tdT) and MHC class II (MHCII-tdT) protein expression[9]. In line with published literature, Olig2 staining was less intense in the aging CNS than the young adult or neonatal CNS, reflecting that the aged CNS contains fewer OPCs and more mature oligodendrocytes than the young CNS[21]. We observed Olig2 + tdT + cells in the ventral brain (Fig. 1A) and in the lumbar spinal cord (Fig. 1B) of B2M-tdT mice at all ages. In the brain of MHCI-tdT mice, there were fewer Olig2 + tdT + cells in aging mice than in young adults, but no differences between neonatal and young adult mice. In the spinal cord, there was a higher percentage of Olig2 + cells co-expressing tdT in young adult mice than in neonates.

In contrast, Olig2 + tdT + cells were not observed anywhere in the brain at any age in MHCII-tdT animals (Fig. 2A) or in the spinal cord of neonatal and young adult animals (Fig. 2B). However, Olig2 + tdT + cells were detected in both the white and gray matter of the lumbar cord of aging animals (Fig. 2C).

IFNγ-AAV system induces focal inflammation that can be compared across ages

Next, we sought to determine if iOPC/OL induction varied with age in an inflammatory context. We previously used $MOG_{35–55}$ induced experimental autoimmune encephalomyelitis (EAE) to explore induction of MHC class I and II molecules in OPCs/OLs[9]. However, this model does not allow for comparison across age groups because the immune system has not fully matured until 8 weeks of age in order to respond to EAE induction[22], and the degree of damage and inflammatory infiltrate in EAE varies with age[23]. In vitro, IFNγ induces MHC expression in oligodendroglia, and we previously showed that ectopic overexpression of IFNγ in astrocytes induces MHC expression in oligodendroglia in vivo[8], but this doxycycline-controlled transgenic model results in neonatal lethality[24]. Therefore, to induce focal inflammation across different age groups, we used an adeno-associated viral (AAV) strategy (Fig. 3A). In brief, we performed unilateral cortical injections of AAV9-GFAP(0.7)-m-IFNγ-IRES-eGFP construct (referred to as IFNγ-AAV hereafter), after which infected astrocytes express IFNγ and eGFP. As a control, we used an eGFP only AAV (eGFP-AAV). p1 pups were injected with 10^{11} vg/mL of IFNγ-AAV or eGFP-AAV in 0.1 µL. Young adult and aging mice were injected following stereotaxic coordinates with 10^{12} vg/mL in 1 µL. Two weeks after injection, brains were collected for analysis.

We first quantified oligodendroglia markers to determine if IFNγ-AAV affected OPC/OL viability or maturity. The density of Olig2 + cells and the intensity of MBP in IFNγ-AAV-injected brains were not significantly different from eGFP-AAV-injected brains (Fig. 3B), indicating that IFNγ-AAV did not result in demyelination or OPC/OL death two weeks after injection. However, there was a significantly lower density of PDGFRα + cells in neonatal IFNγ-AAV injected mice than in eGFP-AAV injected mice (Fig. 3B). Previous studies showed neonatal OLs are more sensitive to IFNγ than adult OLs due to the increased metabolic demands on actively myelinating cells[25]. This suggests that more mature cells might be lost in IFNγ-AAV-injected mice, driving an increase in OPC differentiation to compensate for loss of more mature cells.

Next, we examined the pattern of tdT and eGFP expression in injected brains. In MHCII-tdT animals, tdT signal was seen in focal lesions in the cortices of mice injected with IFNγ-AAV but not eGFP-AAV, (Fig. 3C), demonstrating that the stereotaxic injection itself did not induce MHC class II expression, but that IFNγ-AAV successfully induced inflammation. In MHCI-tdT animals, tdT was visible throughout the brain of eGFP-AAV and IFNγ-AAV-injected animals, as expected (Fig. 3C), but focal regions of increased tdT intensity were observed only with IFNγ-AAV (Fig. 3C). Finally, we confirmed that eGFP colocalized exclusively with GFAP, confirming that our viral constructs specifically transduced astrocytes (Fig. 3D).

MHC class I induction after IFNγ-AAV is consistent across age

Next, we quantified tdT + Olig2 + cells to determine if MHC induction varied with age after AAV injection. Though we controlled for viral titer and the location of injection, we observed differences in AAV diffusion and efficiency across age groups (Supp. Figure). Notably, AAV diffusion and efficiency was highest in neonatal

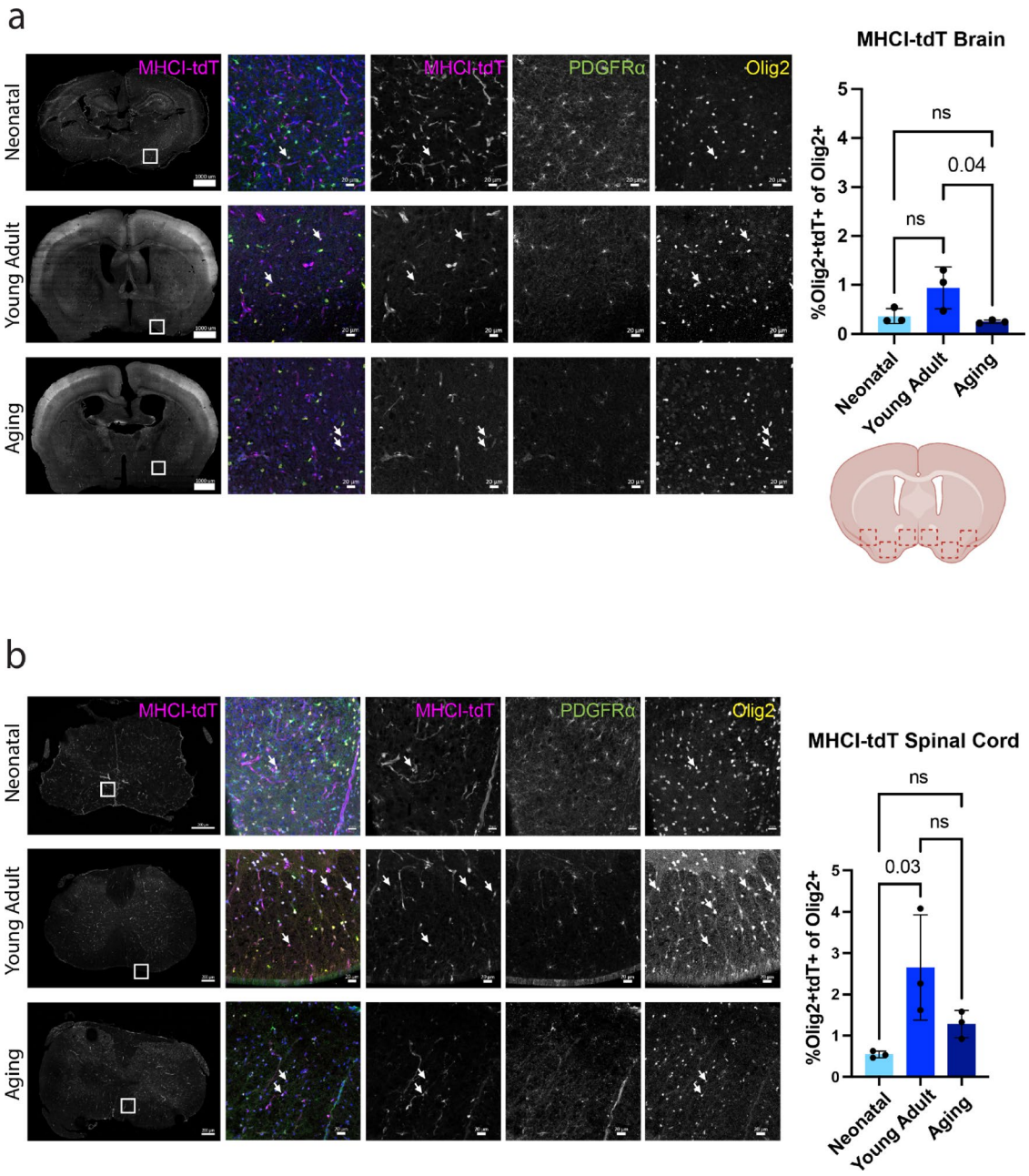

Fig. 1. MHCI-tdT + oligodendroglia are present in the brain and spinal cord of neonatal, young adult, and aging mice. (**a**) Representative images and quantification of Olig2 + tdT + cells in neonatal, young adult, and aging MHCI-tdT brain from 6 ventral regions of interest highlighted in the schematic. In merged images, MHCI-tdT is magenta, PDGFRα is green, Olig2 is yellow, and DAPI is blue. (White squares indicate areas selected for higher magnification in representative images; arrowheads indicate cells co-expressing tdT and Olig2; $N = 3$ animals per group). (**b**) Representative images and quantification of Olig2 + tdT + cells in neonatal, young adult, and aging whole MHCI-tdT spinal cord. In merged images, MHCI-tdT is magenta, PDGFRα is green, Olig2 is yellow, and DAPI is blue. (White squares indicate areas selected for higher magnification in representative images; arrowheads indicate cells co-expressing tdT and Olig2; $N = 3$ animals per group). For a and b, graphs show mean ± standard deviation of each experimental group and groups were statistically compared to each other using one-way ANOVA followed by Tukey's multiple comparisons. Numbers above brackets represent significant p-values; *ns* not significant.

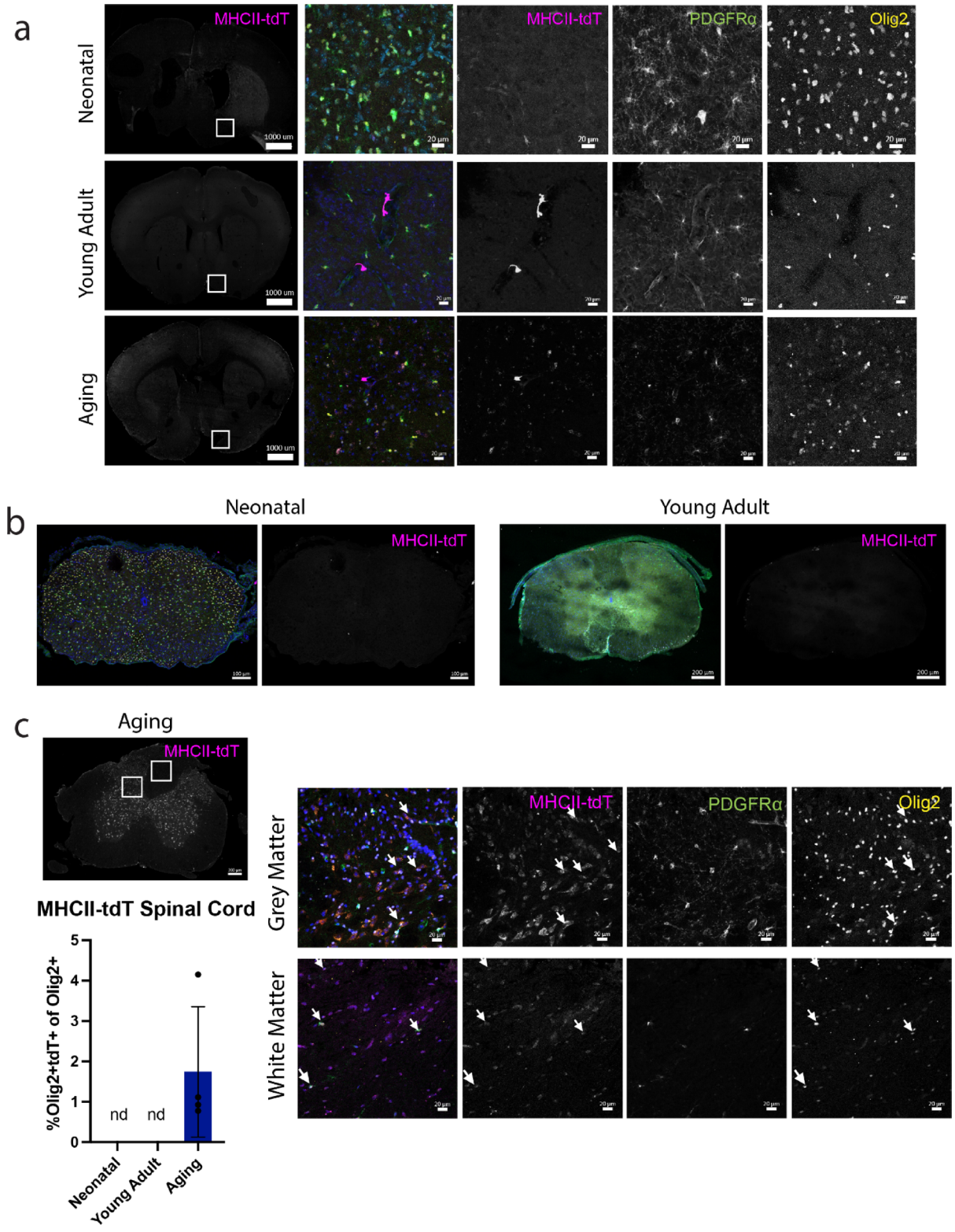

Fig. 2. MHCII-tdT + oligodendroglia are specific to the aging spinal cord. (**a**) Representative images of Olig2 staining in neonatal, young adult and aging MHCII-tdT brain shows no colocalization with tdT. In merged images, MHCII-tdT is magenta, PDGFRα is green, Olig2 is yellow, and DAPI is blue. (**b**) Representative images of MHCII-tdT spinal cords from neonatal and young adult animals showing no tdT signal. In merged images, MHCII-tdT is magenta, PDGFRα is green, Olig2 is yellow, and DAPI is blue. (**c**) Representative images and quantification of Olig2 + tdT + cells in aging MHCII-tdT spinal cord grey and white matter. In merged images, MHCII-tdT is magenta, PDGFRα is green, Olig2 is yellow, and DAPI is blue. White squares indicate areas selected for higher magnification; arrowheads indicate cells co-expressing tdT and Olig2; *nd* not detected; $N = 3–4$ animals per group.

animals, consistent with previously published results[26–28]. As both the number of IFNγ-expressing cells and their proximity would affect the levels of IFNγ that a given OPC/OL would be exposed to, we needed to control for differences in transduction efficiency to compare across age groups. We did this by normalizing our quantification of Olig2 + tdT + cells to the density of GFP + cells in the region of interest.

In MHCI-tdT animals, tdT intensity was increased in IFNγ-AAV-injected animals of all ages compared to eGFP-AAV, consistent with the induction of inflammation, but overall tdT intensity was not different between the age groups (Fig. 4B). We observed Olig2 + tdT + cells in both IFNγ-AAV and eGFP-AAV-injected animals (Fig. 4A). There was no difference in the abundance of Olig2 + cells expressing tdT after IFNγ-AAV between age groups and similarly, there was no difference in the tdT intensity in individual Olig2 + cells (Fig. 4C), demonstrating that both the quantity of cells expressing MHC class I and the levels of MHC class I induced were consistent across ages.

Finally, we quantified the distance between individual Olig2 + tdT + cells and the edge of the nearest GFP + cell, assuming that cells further away from transduced astrocytes are exposed to less IFNγ, and thus might have a lower threshold for MHC induction. Our spatial analysis revealed that a greater proportion of the neonatal Olig2 + tdT + cells were located more than 50 μm from the nearest GFP + cell, and a smaller proportion were less than 50 μm than in young adult or aging mice. This suggests neonatal iOPC/OL may have a higher sensitivity to IFNγ allowing them to be further from the source of inflammation (Fig. 4D).

MHC class II induction after IFNγ-AAV is elevated in aging animals

In MHCII-tdT animals, tdT expression was not detected in eGFP-AAV injected brains. IFNγ-AAV-injected induced robust tdT signal. The overall tdT intensity was not significantly different in animals of different ages, indicating that the overall inflammatory response to IFNγ-AAV was comparable (Fig. 5B). Olig2 + tdT + cells were present inMHCII-tdT brains injected with IFNγ-AAV (Fig. 5A). While CD74-tdT was induced in Olig2 + cells in mice from all three age groups, Olig2 + tdT + cells were more abundant in aging mice than in neonates and young adults after IFNγ exposure (Fig. 5C). This mirrors the trend seen in the MHCII-tdT spinal cord at baseline. Importantly, the percentage of Iba1 + tdT + cells was constant across age (Fig. 5D), indicating that this trend is specific to Olig2 + cells. In addition, the intensity of the tdT signal in Olig2 + cells did not vary with age (Fig. 5C), illustrating that while the number of cells that upregulate MHC class II increases with aging, the degree of CD74 induction in Olig2 + cells is constant. Lastly, no significant difference was observed between the age groups in the spatial analysis (Fig. 5E).

Discussion

In summation, we observed that MHC class II, but not class I, expression varies with age in oligodendroglia. At baseline, MHC class I-expressing OPC/OLs are present in the brain and spinal cord across all age groups analyzed. MHC class II-expressing oligodendroglia, in contrast, were specific to the aging spinal cord. IFNγ-AAV produced inflammation and induction of oligodendroglial MHC, indicating that it recapitulates iOPC/OL pathology observed in EAE in a focal manner that can be compared across ages. IFNγ exposure in the brain induced MHC class I and II expression in Olig2 + cells in mice of all ages, but MHC class II-expressing oligodendroglia were more prevalent in aging animals, while no age differences were seen with MHC class I.

The difference in age sensitivity between MHC class I and II may be driven by their distinct transcriptional regulators. MHC class II induction requires class II MHC transactivator (CIITA) expression in addition to transcription factors and enhancers. As oligodendroglia are not professional antigen presenting cells, induction of CIITA occurs via promoter IV, which uniquely requires binding of interferon response factors, USF-1, and STAT1[29]. Transcriptional regulation of MHC class I has less requirements in comparison, which may be less sensitive to aging[30]. Additional research is needed to determine the mechanism underlying age-related differences in MHC class II induction in oligodendroglia. It likely involves a combination of intrinsic and extrinsic factors. MHC suppression in other contexts, such as the tumor microenvironment, often involves chromatin remodeling[31]. Alternatively, upregulation of MHC class II in aging mice might reflect increased basal levels of inflammation associated with aging, supported by our observation of CD74-tdT + Olig2 + cells in the naïve aging spinal cord.

Our finding that MHC class I expression did not increase with aging in oligodendroglia differs from previous studies in microglia and neurons, where MHC class I expression is elevated in aged animals[32,33]. Using the same MHC reporter animals, we previously showed that MHC class I-expressing Olig2 + cells are present in the naïve CNS of young adult mice and elevated in mouse models of MS. In contrast, MHC class II-expressing cells were only observed in the disease state[9]. This suggested that MHC class I may play a homeostatic role in oligodendroglia, which is supported by our results here that B2M-tdT + Olig2 + cells are present at baseline in mice of all ages and are induced under inflammatory conditions to similar extents in each of the age groups.

Despite there being no age-related change in the amount of OPC/OL expressing MHC class I after IFNγ exposure, MHC class I-expressing oligodendroglia were located further from eGFP + IFNγ -producing astrocytes in neonatal mice compared to young adult and aging animals. This suggests that the neonatal oligodendroglia might be more sensitive to IFNγ, allowing MHC induction to occur further from the stimulus. This observation

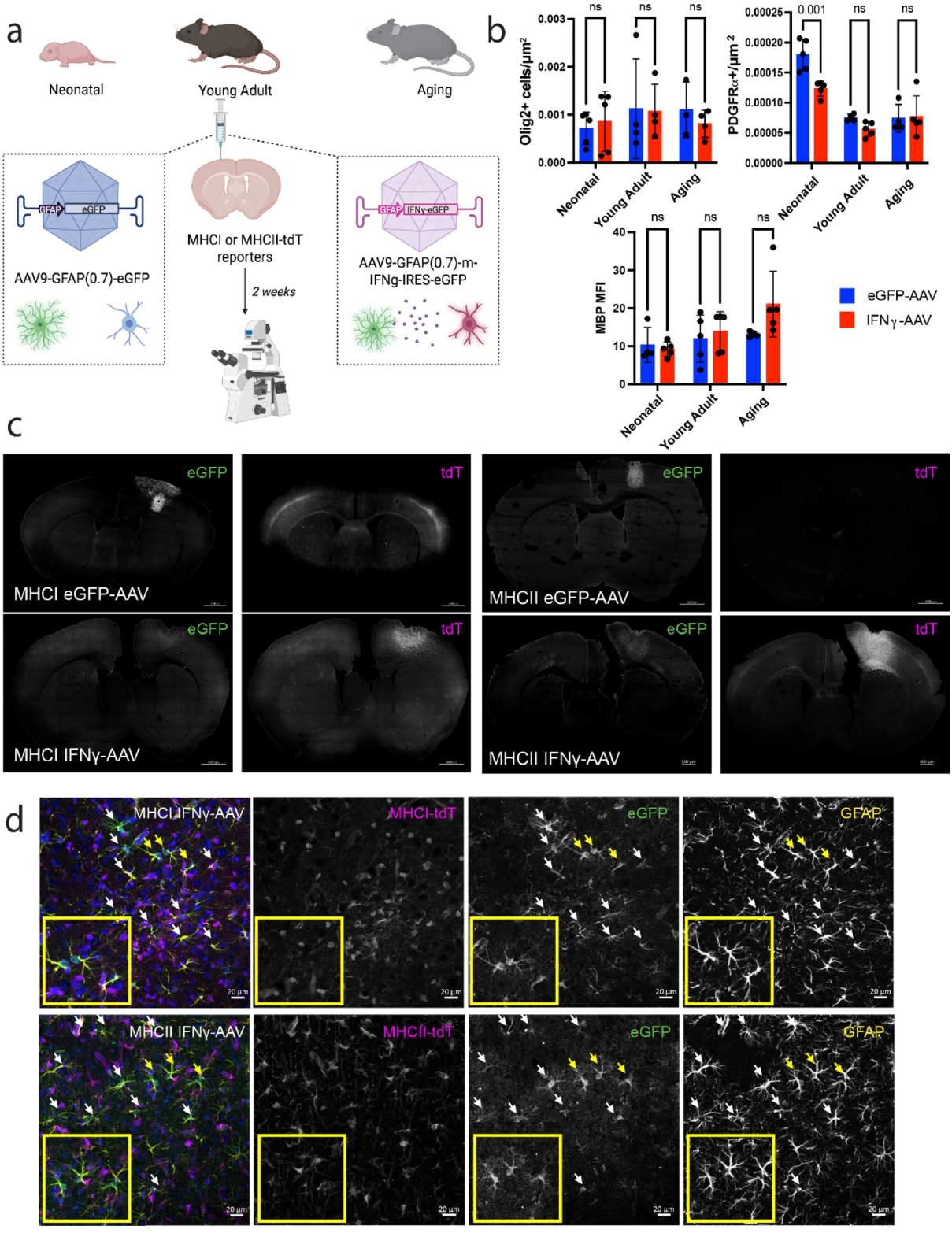
a
Neonatal
Young Adult
Aging
GFAP
eGFP
AAV9-GFAP(0.7)-eGFP
MHCI or MHCII-tdT reporters
2 weeks
GFAP
IFNγ-eGFP
AAV9-GFAP(0.7)-m-IFNg-IRES-eGFP
b
Olig2+ cells/µm²
PDGFRα+/µm²
MBP MFI
ns
0.001
Neonatal
Young Adult
Aging
eGFP-AAV
IFNγ-AAV
c
eGFP
tdT
MHCI eGFP-AAV
MHCII eGFP-AAV
MHCI IFNγ-AAV
MHCII IFNγ-AAV
d
MHCI IFNγ-AAV
MHCI-tdT
eGFP
GFAP
MHCII IFNγ-AAV
MHCII-tdT
20 µm

◀**Fig. 3**. IFNγ-AAV induces focal inflammation and specifically transduces GFAP + astrocytes. (**a**) Schema of AAV experiment methods. eGFP-AAV or IFNγ-AAV was injected unilaterally into the cortex of neonatal, young adult, or aging mice. Two weeks after injection, tissue was collected for analysis by immunohistochemistry. Figure made with BioRender. (**b**) Quantification of Olig2 and PDGFRα density and MBP mean fluorescence intensity (MFI) in eGFP-AAV and IFNγ-AAV-injected neonatal, young adult, and aging brains in the region of interest ($N = 3–5$ animals per group). (**c**) Representative images of eGFP-AAV and IFNγ-AAV-injected brains in MHCI-tdT and MHCII-tdT brains showing GFP and tdT are located in the same area and IFNγ-AAV but not eGFP-AAV increases tdT expression. (**d**) Representative images of GFAP staining in young adult MHCI-tdT and MHCII-tdT IFNγ-AAV-injected brains showing colocalization of GFP with GFAP. In merged images, tdT is magenta, eGFP is green, GFAP is yellow, and DAPI is blue. Arrowheads indicate cells co-expressing GFAP and GFP, and yellow arrowheads indicate cells enlarged in inset shown in yellow boxes. For (**b**), groups were compared using two-way ANOVA followed by Šidák's multiple comparisons test. Graphs show mean ± standard deviation of each experimental group. Numbers above brackets represent significant p-values; *ns* not significant.

is in line with published literature showing differential expression of inflammatory genes between pediatric and adult oligodendroglia. A study of human OLs showed that cells from pediatric brains expressed higher levels of inflammatory genes than adult cells, including B2M and MHC class I HLA-A, B, and C[34]. When they further subdivided pediatric samples into age groups, they found that this effect was primarily driven by cells from patients younger than 5 years old. These data suggest a short period in which MHC class I-expressing iOLs are more abundant in pediatric than adult individuals. The same group demonstrated that interferon response factors and the cellular response to cytokine signaling pathway were more active in pediatric OPCs than adult[35]. Neonatal OPC/OL ability to upregulate MHC class I in response to inflammation could have implications for developmental neurological diseases. White matter abnormalities are present in autism spectrum disorder[36], which is associated with both prenatal maternal immune activation and MHC genetic variants[37]. Additionally, young children are known to be at higher risk of neuroinfection than adults due to immature peripheral immunity[38]. Infection at these stages result in long-term effects on the CNS, given the disruption to ongoing CNS development[39], and oligodendroglia may be primed to respond to signs of infection during early CNS development.

We showed, on the other hand, that MHC class II-expressing oligodendroglia are specific to inflamed contexts and the aging spinal cord. As our aging mice were meant to correspond to PMS age of onset, these results have clinical implications. MHC class II, but not MHC class I, haplotype has long been known to have a strong genetic association with MS risk[40]. Some evidence suggests MHC class II haplotype may be associated with MS progression specifically. In African American patients with MS, *HLA-DRB1*1503* in the absence of *HLA-DRB5* is associated with increased risk of transition to secondary SPMS[41]. In a cohort of nearly 300 Caucasian German MS patients, *HLA-DRB1*1501* haplotype was associated with increased frequency of SPMS[42]. In addition, accelerated epigenetic aging has been shown in white matter of MS patients compared to healthy controls[43], suggesting that oligodendroglia in patients may be primed for increased MHC class II induction. Comparisons of RRMS and PMS tissue can reveal if MHC class II-expressing iOPC/OLs are more abundant in the later phase of disease or more abundant than in age-matched controls. Beyond MS, iOPC/OLs have been described in other aging-associated neurodegenerative diseases such as Alzheimer's disease, where white matter abnormalities are also present[44], raising the possibility that iOPC/OLs play a part in driving white matter abnormalities in such contexts.

Several limitations in our approach should be considered. While every attempt was made to keep the injections as comparable as possible across animals and experimental groups, the area and location of AAV transduction varied, particularly in neonates. While we controlled for GFP + cell density, and AAV9 efficiency has been shown to be comparable in aged and young adult animals when directly injected into the brain[45], we did not account for potential differences in the overall levels of IFNγ after AAV injection.

In conclusion, we demonstrate a specific effect of age on MHC baseline expression and induction in oligodendroglia. These results open future routes of investigation into the role of immune oligodendroglia in development, aging, and neuroinflammatory disease.

Materials and methods

Mice

All animal procedures were performed according to protocols approved by the Johns Hopkins Animal Care and Use Committee. C57BL/6J (Jackson 000644) mice were obtained from Jackson Laboratories. MHCI (B2M-tdT; Jackson 039410)) and MHCII (CD74-tdT; Jackson 039411) reporter mice were established as previously described[9]. Male and female mice were used for all experiments. This study is performed in accordance with relevant guidelines and regulations. All methods are reported in accordance with ARRIVE guidelines.

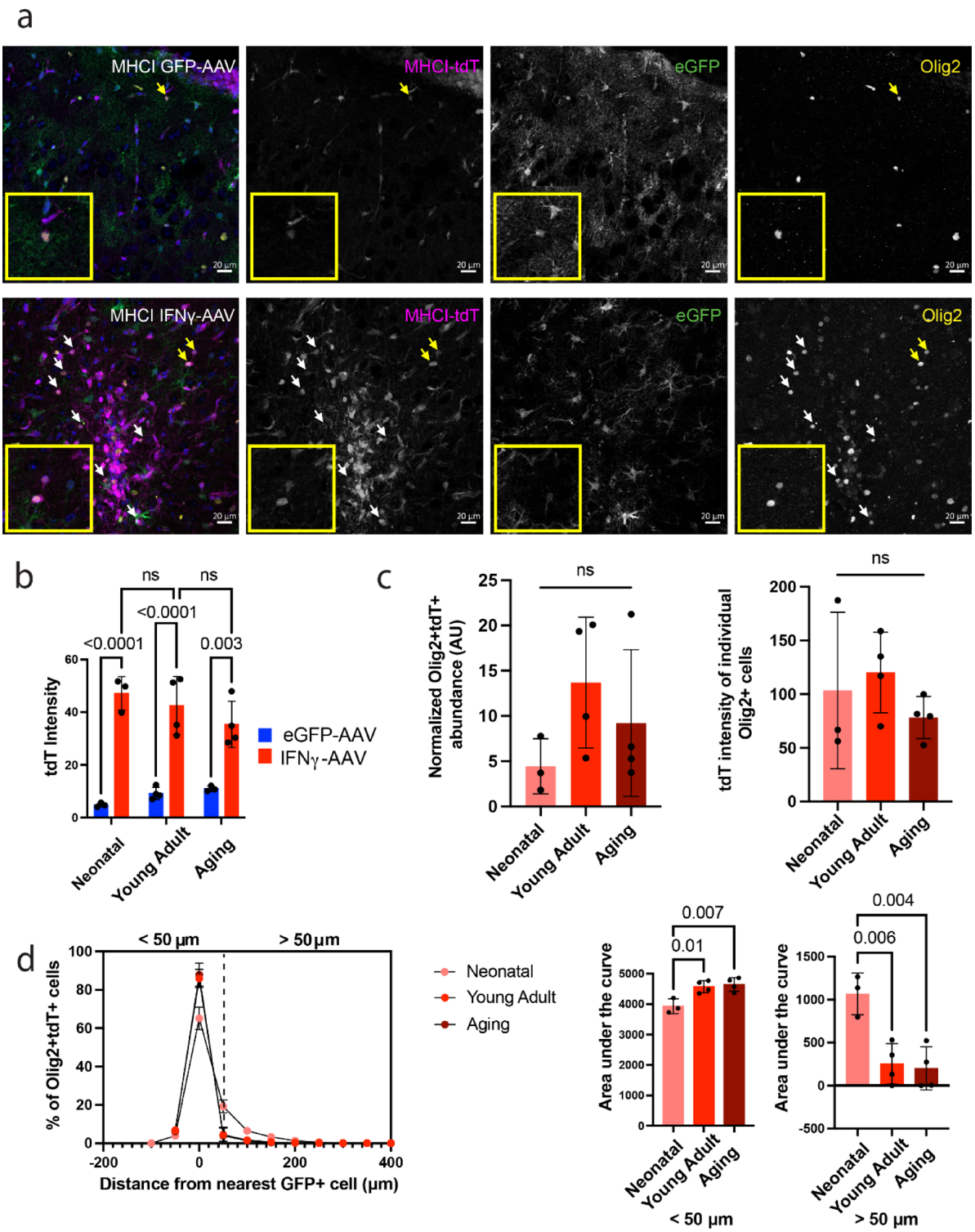

Fig. 4. MHCI-tdT + Olig2 + cell prevalence does not vary with age after AAV injection. (**a**) Representative images of Olig2 + tdT + cells in eGFP-AAV and IFNγ-AAV-injected MHCI-tdT young adult brains. In merged images, MHCI-tdT is magenta, eGFP is green, Olig2 is yellow, and DAPI is blue. Arrowheads indicate cells co-expressing tdT and Olig2, and yellow arrowheads indicate cells enlarged in inset shown in yellow box. (**b**) Quantification of total ROI tdT intensity in eGP-AAV and IFNγ-AAV-injected MHCI-tdT neonatal, young adult, and aging brains ($N = 3–5$ animals per group). (**c**) Quantification of the normalized Olig2 + tdT + abundance ((%tdT + of Olig2+/(GFP+/µm^2))/10,000) and the tdT intensity of individual Olig2 + tdT + cells in IFNγ-AAV-injected MHCI-tdT animals ($N = 3–5$ animals per group). (**d**) Frequency distribution and area under the curve of the percentage of Olig2 + tdT + cells found at binned distances from the closest GFP + cell. (**b**, **c**) two-way ANOVA followed by Tukey's multiple comparisons; (**d**) one-way ANOVA followed by Tukey's multiple comparisons; graphs show mean ± standard deviation of each experimental group. Numbers above brackets represent significant p-values; *ns* not significant, *AU* arbitrary units.

Immunohistochemistry

Mice were anesthetized with isoflurane and perfused intracardially with ice cold PBS followed by 4% PFA. Brain and spinal cord were removed and fixed overnight in 4% PFA, then washed in PBS and transferred to 30% sucrose for 48 h. Tissue was embedded in OCT (TissueTek) and frozen on dry ice. Tissue was cut on Leica CM1850 cryostat and spinal cord 30 µm sections were mounted onto slides and brain 20 µm sections were collected in cryoprotectant (30% sucrose, 30% ethylene glycol, 10 mg/mL polyvinylpyrrolidone in 0.1 M PB buffer pH 7.4–10.9 mg/ml Na_2PO_4, 3.2 mg/ml NaH_2PO_4 in dH_2O). Floating sections were stored at −20 °C and mounted sections were stored at −80 °C. Floating sections were mounted onto slides prior to staining and allowed to dry for 10 min. Slides were washed 3 times for 5 min in PBS, permeabilized in Triton 0.5% in PBS (PBST) for 5 min and blocked for 1 h in 5% normal donkey serum in PBST at room temperature. Cells were then incubated overnight at 4 °C in primary antibodies (rabbit PDGFRα 1:500 (Cell Signaling 3174 S), goat Olig2 1:100 (R&D Systems AF2418), rabbit Olig2 1:1000 (Millipore AB9610), rabbit Iba1 1:1000 (Wako 019-19741), mouse MBP 1:2000 (BioLegend 808402), chicken GFP 1:100 (Aves Labs GFP1010) in PBST with serum. Cells were washed with PBST for 5 min and incubated in secondary antibodies (all used at 1:500) in PBST + serum for 1 h at room temperature (donkey anti-rabbit 488 (Thermo Scientific A31572), donkey anti-goat 647 (Jackson ImmunoResearch 705-605-147), donkey anti-chicken 488 (Jackson ImmunoResearch 703-545-155), donkey anti-mouse 647 (Jackson ImmunoResearch 715-605-150), donkey anti-rabbit 647 (Jackson ImmunoResearch 711-605-152)). Cells were washed for 5 min in PBS, incubated in DAPI (0.5 ng/mL) in PBS for 10 min, washed 3 more times in PBS, and mounted with Prolong Glass Antifade Mountant (Thermo Scientific P36984).

Imaging and quantification

Images were taken on Zeiss LSM 900 confocal. For quantification of naïve tissue, tiled, z-stack 20X images were taken of 4 lumbar spinal cord sections or brain slices (approximately 0.5 and 1 mm anterior to bregma and 0.5 and 1 mm posterior) per mouse. For the spinal cord, entire sections were imaged, while for brain, 6 ROIs were selected from the lateral and medial ventral brain grey matter, bilaterally, for each section. Olig2 + TdT + cells were manually quantified in Zen Blue and total Olig2 + cell counts were made using ImageJ. For AAV-injected tissues, 3 brain sections surrounding the injection area were imaged per animal. A region of interest was defined based on the presence of eGFP + cells; the entire region of the brain containing eGFP + cells was outlined. Within the ROI, Olig2 + TdT + were quantified manually in Zen Blue. Intensity values for both individual cells and the entire ROI were also obtained from Zen Blue. Automated total cell counts were done in ImageJ. The normalized Olig2 + tdT + abundance in AAV-injected brains was calculated as follows: (%tdT + of Olig2+/(GFP+/μm^2))/10,000. For Iba1 + tdT analysis, the spot function in Imaris 10.1 was used to identify total Iba + cells and colocalization with tdT. For spatial Olig2 + tdT + analysis, the spots function was used to identify Olig2 + tdT + cells and the surfaces function was used to identify GFP + cells. The software was then used to calculate the shortest distance between the center of each Olig2 + tdT + cell and the edge of the nearest GFP + cell.

AAV injections

AAV9-GFAP(0.7)-m-IFNγ-IRES-eGFP (AAV-261933) and AAV9-GFAP(0.7)- eGFP (VB1149) were obtained from Vector BioLabs. P1 pups were placed on ice until anesthetized. A 34-gauge needle was used to inject 10^{11} vg/mL in 0.1 µl in one hemisphere, approximately 1 mm lateral of bregma. For the young adult and aged groups, mice were anesthetized with isoflurane and placed in a stereotaxic frame (Stoelting, Wood Dale, IL, USA). Virus injections were performed with a 34-gauge needle attached to a 10µL Hamilton syringe at a rate of 0.5µL/min. Each vector-treated mouse received 1 µL of the vector of either AAV9-GFAP(0.7)- eGFP (10^{11} vg/mL) or AAV9-GFAP(0.7)-m-IFNγ-IRES-eGFP (10^{11} vg/mL). The coordinates for injections were: 1 mm anterior to bregma, 1.5 mm lateral and 0.8 mm under dura. Following the injection, the needle was left in place an additional 2 min before being slowly removed from the brain. Mice were dosed with SR-buprenorphine (0.5 mg/kg) before being removed from the isoflurane anesthesia and returned to their home cages.

Statistical analysis

Two-tailed t-test analysis, one-way ANOVA corrected for multiple comparisons with Tukey's test or two-way ANOVA corrected for multiple comparisons with Šidák's test were performed as indicated in the figure legends, using GraphPad Prism 9. In all figure legends, N refers to the number of independent experiments. Significance level was set at $p < 0.05$.

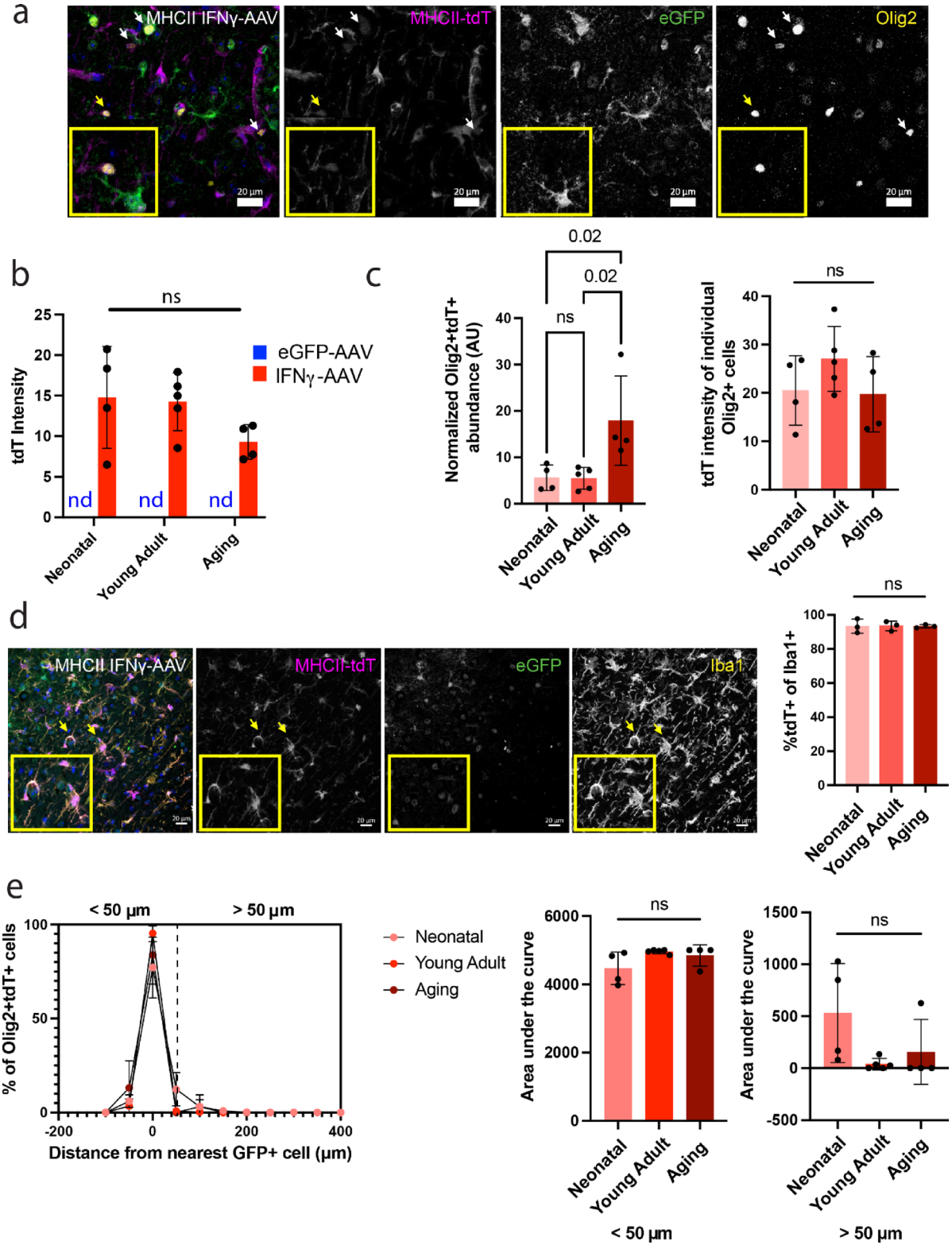
a
MHCII IFNγ-AAV
MHCII-tdT
eGFP
Olig2
20 µm
b
ns
tdT Intensity
eGFP-AAV
IFNγ-AAV
nd
nd
nd
Neonatal
Young Adult
Aging
c
0.02
0.02
ns
Normalized Olig2+tdT+ abundance (AU)
Neonatal
Young Adult
Aging
ns
tdT intensity of individual Olig2+ cells
Neonatal
Young Adult
Aging
d
MHCII IFNγ-AAV
MHCII-tdT
eGFP
Iba1
ns
%tdT+ of Iba1+
Neonatal
Young Adult
Aging
e
< 50 µm
> 50 µm
% of Olig2+tdT+ cells
Distance from nearest GFP+ cell (µm)
Neonatal
Young Adult
Aging
ns
Area under the curve
Neonatal
Young Adult
Aging
< 50 µm
ns
Area under the curve
Neonatal
Young Adult
Aging
> 50 µm

◀**Fig. 5**. MHC class II induction is higher in oligodendroglia of aging mice than neonatal and young adult mice after IFNγ-AAV injection. (**a**) Representative images of Olig2 + tdT + cells in IFNγ-AAV-injected MHCII-tdT young adult brain. In merged image, MHCII-tdT is magenta, eGFP is green, GFAP is yellow, and DAPI is blue. Arrowheads indicate cells co-expressing tdT and Olig2, and yellow arrowheads indicate cells enlarged in inset shown in yellow box. (**b**) Quantification of total ROI tdT intensity in IFNγ-AAV-injected MHCII-tdT brains ($N = 4–5$ animals per group; nd: not detected). (**c**) Quantification of the normalized Olig2 + tdT + abundance ((%tdT + of Olig2+/(GFP+/μm^2))/10,000) and the tdT intensity of individual Olig2 + tdT + cells in IFNγ-AAV-injected MHCII-tdT animals ($N = 4–5$ animals per group). (**d**) Representative staining and quantification of Iba1 colocalization with tdT in MHCII-tdT IFNγ-AAV-injected brain ($N = 3$ animals per group). In merged image, MHCII-tdT is magenta, eGFP is green, Iba1 is yellow, and DAPI is blue. (**e**) Frequency distribution and area under the curve of the percentage of Olig2 + tdT + cells found at binned distances from the closest GFP + cell ($N = 4–5$ animals per group). For (**b–e**), groups were statistically compared to each other using one-way ANOVA followed by Tukey's multiple comparisons; graphs show mean ± standard deviation of each experimental group. Numbers above brackets represent significant p-values; *ns* not significant, *AU* arbitrary units.

Data availability

The datasets used and/or analyzed during the current study are available from the corresponding author on reasonable request and with permission from JHU Office of Technology Licensing.

Received: 16 November 2024; Accepted: 19 May 2025
Published online: 26 May 2025

References

1. Graves, J. S. et al. Ageing and multiple sclerosis. *Lancet Neurol.* **22**, 66–77 (2023).
2. Capasso, N. et al. Aging in multiple sclerosis: from childhood to old age, etiopathogenesis, and unmet needs: a narrative review. *Front. Neurol.* **14**, 1 (2023).
3. Hagemeier, K., Brück, W. & Kuhlmann, T. Multiple sclerosis–remyelination failure as a cause of disease progression. *Histol. Histopathol.* **27**, 277–287 (2012).
4. Bramow, S. et al. Demyelination versus remyelination in progressive multiple sclerosis. *Brain* **133**, 2983–2998 (2010).
5. Sim, F. J., Zhao, C., Penderis, J. & Franklin, R. J. M. The age-related decrease in CNS remyelination efficiency is attributable to an impairment of both oligodendrocyte progenitor recruitment and differentiation. *J. Neurosci.* **22**, 2451–2459 (2002).
6. Sams, E. C. Oligodendrocytes in the aging brain. *Neuronal Signal.* **5**, NS20210008 (2021).
7. Segel, M. et al. Niche stiffness underlies the aging of central nervous system progenitor cells. *Nature* **573**, 130 (2019).
8. Kirby, L. et al. Oligodendrocyte precursor cells present antigen and are cytotoxic targets in inflammatory demyelination. *Nat. Commun.* **10**, 1–20 (2019).
9. Harrington, E. P. et al. MHC class i and MHC class Ii reporter mice enable analysis of immune oligodendroglia in mouse models of multiple sclerosis. *Elife* **12**, 1 (2023).
10. Jäkel, S. et al. Altered human oligodendrocyte heterogeneity in multiple sclerosis. *Nature* **566**, 543–547 (2019).
11. Falcão, A. M. et al. Disease-specific oligodendrocyte lineage cells arise in multiple sclerosis. *Nat. Med.* **24**, 1837–1844 (2018).
12. Absinta, M. et al. A lymphocyte–microglia–astrocyte axis in chronic active multiple sclerosis. *Nature* **1**, 1–6. https://doi.org/10.1038/s41586-021-03892-7 (2021).
13. Psenicka, M. W., Smith, B. C., Tinkey, R. A. & Williams, J. L. Connecting neuroinflammation and neurodegeneration in multiple sclerosis: are oligodendrocyte precursor cells a nexus of disease? *Front. Cell. Neurosci.* **15**, 654284 (2021).
14. Spitzer, S. O. et al. Oligodendrocyte progenitor cells become regionally diverse and heterogeneous with age. *Neuron* **101**, 459–471 (2019).
15. de la Fuente, A. G. et al. Changes in the oligodendrocyte progenitor cell proteome with ageing. *Mol. Cell. Proteom.* **19**, 1281–1302 (2020).
16. Ximerakis, M. et al. Single-cell transcriptomic profiling of the aging mouse brain. *Nat. Neurosci.* **22**, 1696–1708 (2019).
17. Heo, D. et al. Transcriptional profiles of mouse oligodendrocyte precursor cells across the lifespan. *Nat. Aging 2025.* **54** (5), 675–690 (2025).
18. Dulken, B. W. et al. Single-cell analysis reveals T cell infiltration in old neurogenic niches. *Nature* **571**, 205–210 (2019).
19. Kaya, T. et al. CD8 + T cells induce interferon-responsive oligodendrocytes and microglia in white matter aging. *Nat. Neurosci.* **1**, 1–12. https://doi.org/10.1038/s41593-022-01183-6 (2022).
20. Flurkey, K., Currer, J. M. & Harrison, D. E. Mouse models in aging research. *Mouse Biomed. Res.* **3**, 637–672 (2007).
21. Michalettos, G., Clausen, F., Özen, I., Ruscher, K. & Marklund, N. Impaired oligodendrogenesis in the white matter of aged mice following diffuse traumatic brain injury. *Glia* **72**, 728–747 (2024).
22. Cravens, P. D. et al. The neonatal CNS is not conducive for encephalitogenic Th1 T cells and B cells during experimental autoimmune encephalomyelitis. *J. Neuroinflamm.* **10**, 835 (2013).
23. Atkinson, J. R. et al. Biological aging of CNS-resident cells alters the clinical course and immunopathology of autoimmune demyelinating disease. *JCI Insight* **7** (2022).
24. Lin, W. et al. Interferon-γ induced Medulloblastoma in the developing cerebellum. *J. Neurosci.* **24**, 10074–10083 (2004).
25. Lin, W., Harding, H. P., Ron, D. & Popko, B. Endoplasmic reticulum stress modulates the response of myelinating oligodendrocytes to the immune cytokine interferon-gamma. *J. Cell. Biol.* **169**, 603–612 (2005).
26. Chakrabarty, P. et al. Capsid serotype and timing of injection determines AAV transduction in the neonatal mice brain. *PLoS ONE.* **8**, e67680 (2013).
27. Murlidharan, G., Crowther, A., Reardon, R. A., Song, J. & Asokan, A. Glymphatic fluid transport controls paravascular clearance of AAV vectors from the brain. *JCI Insight.* **1**, e88034 (2016).
28. Sandoval, I. M. et al. Engineered AAV capsid transport mutants overcome transduction deficiencies in the aged CNS. *Mol. Ther. Nucleic Acids.* **35**, 1 (2024).
29. Muhlethaler-Mottet, A., Berardino, W., Di, Otten, L. A. & Mach, B. Activation of the MHC class II transactivator CIITA by interferon-γ requires cooperative interaction between Stat1 and USF-1. *Immunity* **8**, 157–166 (1998).
30. van den Elsen, P. J. Expression regulation of major histocompatibility complex class I and class II encoding genes. *Front. Immunol.* **2**, 15473 (2011).

31. Tomasi, T. B. et al. MHC class II regulation by epigenetic agents and MicroRNAs. *Immunol. Res.* **46**, 45 (2010).
32. Kellogg, C. M. et al. Microglial MHC-I induction with aging and Alzheimer's is conserved in mouse models and humans. *BioRxiv*. https://doi.org/10.1101/2023.03.07.531435 (2023).
33. Starkey, H. D. V. et al. Neuroglial expression of the MHCI pathway and PirB receptor is upregulated in the hippocampus with advanced aging. *J. Mol. Neurosci.* **48**, 111 (2012).
34. Yaqubi, M. et al. Regional and age-related diversity of human mature oligodendrocytes. *Glia*. https://doi.org/10.1002/glia.24230 (2022).
35. Luo, J. X. X. et al. Human oligodendrocyte myelination potential; relation to age and differentiation. *Ann. Neurol.* **91**, 178–191 (2022).
36. Cheng, Y. et al. Atypical development of white matter microstructure in adolescents with autism spectrum disorders. *Neuroimage* **50**, 873–882 (2010).
37. Needleman, L. A. & Mcallister, A. K. The major histocompatibility complex and autism spectrum disorder. *Dev. Neurobiol.* **72**, 1288 (2012).
38. Kim, J., Erice, C., Rohlwink, U. K. & Tucker, E. W. Infections in the developing brain: the role of the neuro-immune axis. *Front. Neurol.* **13**, 805786 (2022).
39. Mwaniki, M. K., Atieno, M., Lawn, J. E. & Newton, C. R. J. C. Long-term neurodevelopmental outcomes after intrauterine and neonatal insults: a systematic review. *Lancet* **379**, 445 (2012).
40. Martin, R., Sospedra, M., Eiermann, T. & Olsson, T. Multiple sclerosis: doubling down on MHC. *Trends Genet.* **37**, 784–797 (2021).
41. Caillier, S. J. et al. Uncoupling the roles of HLA-DRB1 and HLA-DRB5 genes in multiple sclerosis. *J. Immunol.* **181**, 5473–5480 (2008).
42. Stürner, K. H. et al. Is multiple sclerosis progression associated with the HLA-DR15 haplotype? *Mult Scler. J. Exp. Transl Clin.* **5**, 1 (2019).
43. Windener, F. et al. Physiological aging and inflammation-induced cellular senescence May contribute to oligodendroglial dysfunction in MS. *Acta Neuropathol. 2024*. **147**, 1–19 (2024).
44. Lau, S. F., Cao, H., Fu, A. K. Y. & Ip, N. Y. Single-nucleus transcriptome analysis reveals dysregulation of angiogenic endothelial cells and neuroprotective glia in Alzheimer's disease. *Proc. Natl. Acad. Sci. U. S. A.* **117**, 25800–25809 (2020).
45. Gombash, S. E. et al. AAV9 transduction is similar in adult and aged mouse brains following intraparenchymal injection. *Mol. Ther.* **24**, S245 (2016).

Acknowledgements

This work was supported by funding from National Institutes of Health RO1 NS041435 (PAC) and NSF Graduate Research Fellowship (RBC).

Author contributions

RBC designed experiments, conducted experiments, analyzed data, interpreted data, and wrote the manuscript and designed figures. DG designed and conducted experiments and interpreted data. AR and SP conducted experiments and analyzed data. PAC supervised the work, interpreted data, and obtained funding. All authors contributed to editing the final manuscript.

Declarations

Competing interests

PAC is PI on grants to JHU from Genentech and the Myelin Repair Foundation, and has received personal consulting Honoria from Idorsia, Spolia Therapeutics, Novartis, and Lilly. The other authors have no competing interests to declare.

Additional information

Supplementary Information The online version contains supplementary material available at https://doi.org/10.1038/s41598-025-03089-2.

Correspondence and requests for materials should be addressed to P.A.C.